Nano Carbons 2024; 2(1): 1142.
Original Research Article

Resistance of HVOF-Sprayed Cr_3C_2-25NiCr and WC-10CO-4Cr coatings to cavitation and erosion by mud jetting

Androw D. H.[1], Ratchagaraja Dhairiyasamy[2,*]

[1] *Department of Mechanical Engineering, St.Joseph's College of Engineering, OMR, Chennai 600119, India*

[2] *Department of Mechanical Engineering, College of Engineering and Technology, Aksum University, Aksum 1010, Ethiopia*

*** Corresponding author:** Ratchagaraja Dhairiyasamy, ratchagaraja@gmail.com

ARTICLE INFO

Received: 4 March 2024
Accepted: 18 March 2024
Available online: 15 April 2024

doi: 10.59400/n-c.v2i1.1142

ABSTRACT: This study investigates chromium carbide-based coating material's cavitation and erosion resistance with 25% nickel-chromium. (Cr_3C_2-25NiCr) and tungsten carbide coating with 10% cobalt and 4% chromium (WC-10CO-4Cr) coatings deposited by high-velocity oxygen fuel (HVOF) thermal spraying. The coatings were characterized by microstructure, porosity, hardness, and fracture toughness. Cavitation tests were performed in distilled water and water-sand mixtures to assess the synergistic effect of erosion and cavitation. Erosion tests were conducted using a mud jet at different impact angles (30°, 60°, 90°). The Cr_3C_2-25NiCr coating exhibited higher cavitation resistance due to its higher fracture toughness and lower porosity. However, the WC-10CO-4Cr coating showed superior erosion resistance, attributed to its finer and more homogeneously distributed carbides. The dominant wear mechanisms were micro grooving, carbide detachment, and cracking. The impact angle significantly influenced the erosion rates, with ductile materials like CA6NM steel being more susceptible at lower angles, while brittle coatings showed the opposite behavior. The findings highlight the importance of coating properties and test conditions on the wear performance, providing valuable insights for selecting suitable coatings for hydropower applications.

KEYWORDS: HVOF thermal spraying; cavitation resistance; erosion resistance; cermet coatings; wear mechanisms

1. Introduction

Hydropower plants play a crucial role in meeting the global energy demand, but the efficiency and longevity of hydraulic turbines are often compromised by wear phenomena such as cavitation and erosion. Cavitation occurs when rapid pressure changes in the flowing liquid lead to the formation and collapse of vapor bubbles, generating high-impact forces that can damage the turbine components. On the other hand, erosion is caused by the impact of solid particles suspended in the liquid, leading to material removal and surface degradation. These wear mechanisms can significantly reduce the performance and lifespan of hydraulic turbines, resulting in increased maintenance costs and downtime.

Various surface engineering techniques have been employed to mitigate the effects of cavitation and erosion, including applying protective coatings. High-velocity oxy-fuel (HVOF) thermal spraying has emerged as a promising technique for depositing wear-resistant coatings due to its ability to produce dense, well-adhered coatings with low porosity and hardness. Among the commonly used coating

materials, cermet coatings such as Cr_3C_2-NICR and WC-CoCr have garnered attention due to their excellent wear resistance, attributed to hard carbide particles embedded in a tough metallic matrix.

Despite the extensive research on HVOF-sprayed cermet coatings, there is still a need to better understand their performance under complex wear conditions that simulate the environment in hydropower plants. Cavitation and erosion often occur simultaneously, leading to a synergistic effect that can accelerate the wear process. Additionally, the impact angle of the eroding particles can significantly influence the wear mechanisms and rates, with ductile and brittle materials exhibiting different behaviors. Therefore, a comprehensive study investigating hoof-sprayed cermet coatings' cavitation and erosion resistance under various test conditions is crucial for selecting suitable coatings for hydropower applications.

Amarendra et al.[1] studied the combined slurry and cavitation erosion resistance of HVOF-sprayed WC-Co-Cr coatings on stainless steel. Found coatings improved erosion resistance compared to uncoated steel. Ding et al.[2] investigated the structure and cavitation erosion of HVOF sprayed with a WC-Co-Cr coating. Discovered multi-scale structure improved cavitation resistance. Ding et al.[3] examined deposition and cavitation erosion of HVOF-sprayed multimodal WC-Co-Cr coatings. Coating sprayed with liquid fuel had lower porosity and better cavitation resistance. Ding et al.[4] studied the cavitation erosion resistance of HVOF-sprayed WC-Co coatings with multi-scale WC particles. Coating with nano- to micron-sized WC grains showed greatly enhanced cavitation resistance. Hong et al.[5–7] analyzed hydro-abrasive erosion and cavitation-silt erosion of HVOF-sprayed WC-Ni coating. The coating showed higher resistance than steel across flow velocities and sand concentrations. Jonda et al.[8] compared cavitation erosion and wear resistance of HVOF-sprayed WC-CO-CR, WC-Cr_3C_2-Ni, and WC-CO coatings on Mg. WC-CO-CR exhibited the best cavitation resistance due to uniform material removal. Kanno et al.[9] studied the influence of composition, WC grain size, and HVOF spray conditions on cavitation erosion of WC-COCRr and WC-CRC-Ni coatings. Higher combustion pressure improved cohesion and cavitation resistance. Kumar et al.[10,11] HVOF sprayed WC-Co coatings on hydro turbine blades to improve cavitation, erosion, and abrasion resistance. Coatings gave high hardness, abrasion resistance, and cavitation resistance. Lamana et al.[12] investigated the effect of co-content and the HVOF process on cavitation erosion of WC-Co coatings. Higher co-content and liquid fuel use increased fracture toughness and cavitation resistance. Lekatou et al.[13] compared the corrosion and wear behavior of nanostructured and conventional HVOF-sprayed WC-Co-Cr coatings on Al alloy. Nanocoating showed better corrosion and wear resistance. Lin et al.[14] studied cavitation erosion of HVOF-sprayed WC-Ni and WC-Co-Cr coatings in NaCl medium at various flow velocities. Wc-ni coating showed higher cavitation resistance (**Table 1**).

Table 1. Research on the resistance of HVOF-sprayed coatings to erosion and cavitation.

Reference	Objective	Materials	Method	Key Findings
Maekai et al.[15]	Study slurry erosion resistance of HVOF sprayed WC-Co-Cr and Cr_3C_2-Ni coatings on steel.	WC-Co-Cr, Cr_3C_2-Ni coatings on steel	High-speed slurry erosion testing	WC-CO-Cr coating showed superior slurry erosion resistance
Pattnayak et al.[16]	Develop wear and corrosion-resistant Al_2O_3-CeO_2-rGO coatings on steel by HVOF spraying	Al_2O_3-CeO_2-rGO coatings on 17-4 PH steel	Tribological and corrosion testing	rGO addition improved wear resistance and corrosion resistance

Table 1. (*Continued*).

Reference	Objective	Materials	Method	Key Findings
Ribu et al.[17]	Examine slurry erosion performance of HVOF sprayed WC-Co coatings	WC-Co coatings on steel	Slurry erosion testing	Rotational speed is the most significant factor affecting slurry erosion
Ribu et al.[18]	Study influence of parameters on slurry erosion of HVOF sprayed WC-Co coatings.	WC-Co coatings on 35CrMo steel	Slurry erosion testing	Rotational speed is the most significant parameter determining erosion rate.
Shi et al.[19]	Investigate the effect of sulfide on cavitation erosion-corrosion of HVOF sprayed WC-Cr_3C_2-Ni coating.	WC-Cr_3C_2-Ni coating	Cavitation testing in NaCl solutions with sulfide	Sulfide reduced cavitation erosion resistance, and mechanical erosion dominated.
Singh et al.[20]	Evaluate cavitation erosion resistance of HVOF sprayed WC-NiCr and WC-Hastelloy C coatings on Monel alloy.	WC-NiCr and WC-Hastelloy C coatings on Monel K-500	Cavitation testing	WC-NiCr coating reduced erosion loss more than WC-Hastelloy C coating
Singh et al.[21]	Study cavitation erosion mechanisms of HVOF sprayed WC-NiCr and WC-Hastelloy C coatings in NaCl solution.	WC-NiCr and WC-Hastelloy C coatings on Monel K-500	Cavitation-corrosion testing	WC-NiCr coating showed better corrosion resistance and cavitation-corrosion performance.
Singh et al.[22]	Evaluate cavitation erosion of HVOF sprayed VC-CuNiCr coatings on stainless steel.	VC-CuNiCr coatings on SS316 steel	Cavitation testing	VC coating showed excellent cavitation erosion resistance due to hardness and thickness.
Vaz et al.[23]	Review cavitation resistance of FeMnCrSi coatings produced by various thermal spray methods.	FeMnCrSi coatings	Literature review	HVOF and HVAF coatings showed higher cavitation resistance than arc-sprayed coatings
Wei et al.[24]	Examine the effect of WC-Co on cavitation erosion of HVOF-sprayed AlCoCrFeNi coatings.	(AlCoCrFeNi)1-x(WC-Co)x coatings	Cavitation testing	WC-Co slightly increased cavitation resistance by supporting AlCoCrFeNi
Xiao et al.[25]	Develop TiC-reinforced AlCoCrFeNi HEA coating and evaluate properties	TiC/AlCoCrFeNi coating	Microstructure, mechanical testing, wear testing	Dual-sized TiC particles enhanced hardness, toughness, and wear resistance

This research evaluates the performance of HVOF-sprayed Cr_3C_2-25NiCr and WC-10Co-4Cr coatings in resisting cavitation and erosion caused by mud jetting. The study is designed to investigate the coatings thoroughly through several specific objectives. Firstly, it aims to characterize the coatings' microstructure, porosity, hardness, and fracture toughness to establish a foundational understanding of their properties. Secondly, the research seeks to assess the cavitation resistance of these coatings when

exposed to distilled water and water-sand mixtures, thereby exploring the potential synergistic effects of erosion and cavitation on the coatings' durability. Thirdly, the study intends to investigate the coatings' erosion resistance under varying impact angles (30°, 60°, 90°) through a mud jet test, providing insights into how orientation relative to the erosive force affects performance. Finally, by identifying the dominant wear mechanisms and correlating them with the coatings' properties and the test conditions, this research aims to deepen the understanding of how these coatings can be optimized for enhanced resistance to cavitation and erosion in challenging environments. The scope of this study is limited to two HVOF-sprayed cermet coatings, Cr_3C_2-25NiCr and WC-10Co-4Cr, and a reference material, CA6NM steel. The cavitation tests are conducted in distilled water and water-sand mixtures, while the erosion tests are performed using a mud jet at three impact angles (30°, 60°, 90°). The wear mechanisms are characterized using scanning electron microscopy (SEM).

The theoretical framework of this study is based on the concepts of cavitation and erosion wear, as well as the structure-property relationships in cermet coatings. Cavitation wear is governed by the repeated formation and collapse of vapor bubbles, which generate high-impact forces and lead to material removal. Erosion wear is caused by the impact of solid particles, with the wear rates and mechanisms being influenced by the particle characteristics, impact angle, and material properties. The hard carbide particles in cermet coatings provide wear resistance, while the metallic matrix imparts toughness and cohesion. The coating properties, such as hardness, fracture toughness, and porosity, are crucial in determining the wear performance.

2. Materials, methods, and procedure

2.1. Substrate preparation

The substrate material used in this study was SAE 1020 carbon steel, cut into rectangular plates measuring 200 mm × 40 mm × 4.75 mm. Before coating deposition, the substrate surface was grit-blasted using white aluminum oxide with a particle size of 500 μm (36 mesh) to achieve a surface roughness (Ra) of approximately 4 μm. The grit-blasting process was carried out at an air pressure of 551.6 to 620.53 kPa and a blasting distance of 120–150 mm. The grit-blasted samples were then cleaned with compressed air to remove residual grit or debris.

The HVOF thermal spray method deposited the coatings in partnership with the company Revesteel Metalização, located in Pinhais, Paraná. The test used the Diamond Jet - DJ2700 sprinkler system, a model produced by the company METCO, using propane (C3H8) as a gaseous fuel. **Figure 1** shows the HVOF torch and the specimen fixture used.

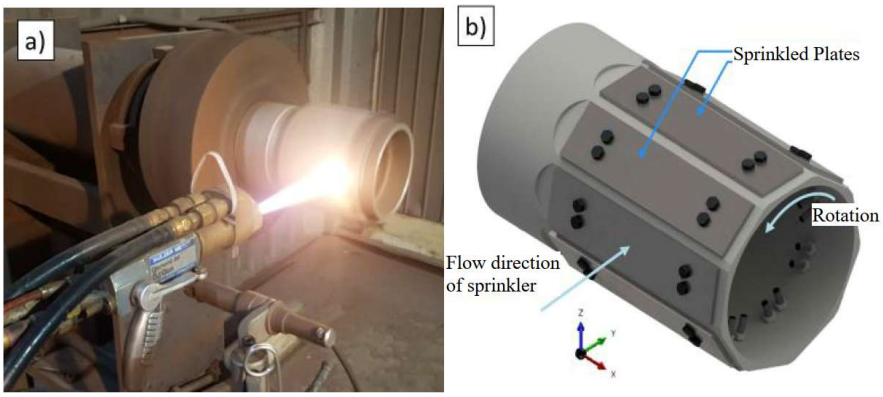

Figure 1. HVOF equipment used in the sprinkler process; **(a)** Diamond Jet DJ2700; **(b)** Specimen clamping device.

Coating deposition:

The Cr_3C_2-25NiCr and WC-10Co-4Cr coatings were deposited using a Diamond Jet DJ2700 HVOF thermal spray system (Oerlikon Metco, USA). The feedstock powders used were WOKA 7205 (Cr_3C_2-25NiCr) and WOKA 3653 (WC-10Co-4Cr), both of which were agglomerated and sintered powders with a nominal particle size range of −45 + 15 μm. The chemical composition of the powders is presented in **Table 2** of the manuscript.

Table 2. Deposition parameters used in HVOF coatings.

Parameter	Specification
Type of Gun	DJ 2700
Oxygen Pressure (MPa)	0.970
Propane Pressure (MPa)	0.560
Nitrogen Pressure (MPa)	0.830
Oxygen Flow (m^3/h)	15.2
Propane Flow (m^3/h)	3.1
Nitrogen Flow (m^3/h)	0.61
Powder feed rate (g/min)	41
Deposition distance (mm)	255

It is important to highlight that the HVOF deposition parameters were chosen based on the optimization carried out by Ribas. This work evaluated the most suitable parameters for wear resistance of Cr_3C_2 25NiCr coatings deposited by HVOF.

In the thermal spray process, two coatings were deposited separately. The first was the Cr_3C_2 25NiCr powder, commercially known as WOKA 7205, which was agglomerated and sintered. The second material was WC powder 10Co-4Cr, known as WOKA 3653, also agglomerated and sintered, both coatings being supplied by the company METCO.

Figure 2 shows the image of the Cr_3C_2 25NiCr powder (WOKA 7205), where it is possible to visualize the chromium carbides in darker tones and the NiCr matrix in lighter tones.

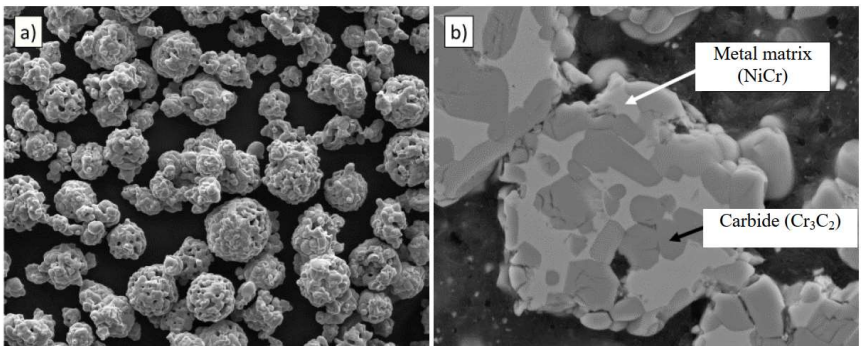

Figure 2. Images of Cr_3C_2 25NiCr powder (WOKA 7205) obtained by Scanning Electron Microscopy; **(a)** 500× magnification; **(b)** Crop view at 3000× magnification.

Based on previous studies, the HVOF spraying parameters were optimized to obtain low porosity and hardness coatings. The spraying parameters used for both coatings are listed in **Table 2** of the manuscript. The coatings were deposited to a thickness of approximately 220–230 μm, as measured using a digital caliper.

2.2. Coating characterization

The as-sprayed coatings were sectioned, mounted in epoxy resin, and polished using standard metallofigureic procedures. The polished cross-sections were examined using a scanning electron microscope with an energy-dispersive X-ray spectroscopy (EDS) system to analyze the coating microstructure and composition.

The porosity of the coatings was evaluated using image analysis techniques. SEM microfigures of the polished cross-sections were acquired at 500× magnification, and the area fraction of porosity was determined using the Image J software, as shown in **Figure 3**.

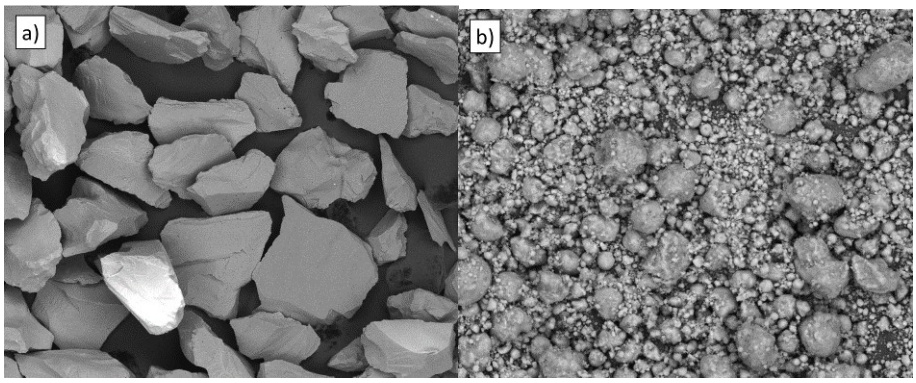

Figure 3. Images of WC 10Co4Cr powder (WOKA 3653) obtained by Scanning Electron Microscopy; **(a)** 500× magnification; **(b)** Crop view at 3000× magnification.

The phase composition of the coatings was investigated using X-ray diffraction (XRD) with a Bruker ECO D8 ADVANCE diffractometer) using Cu-Kÿ radiation (*ÿ* = 1.54 nm). The XRD patterns were acquired over a 2ÿ range of 20°–80° with a step size of 0.04° and a scan speed of 1°/min.

The microhardness of the coatings was measured on the polished cross-sections using a Vickers indenter with a load of 300 gf and a dwell time of 15 s. Ten indentations were made on each coating, and the average microhardness value was reported.

The fracture toughness of the coatings was evaluated using the indentation crack length method. Vickers indentations were made on the polished cross-sections using a higher load of 10 kgf, and the crack lengths emanating from the indentation corners were measured using an optical microscope.

2.3. Cavitation erosion testing

Cavitation erosion tests were performed using an ultrasonic vibratory apparatus (Qsonica Q700, USA) following ASTM G32. The test samples (25 mm × 40 mm × 4.75 mm) were mounted on a stationary specimen holder and immersed in distilled water maintained at a temperature of 25 ± 1 °C. The vibratory horn, with a diameter of 19 mm, was positioned above the sample surface at a distance of 500 µm. The horn vibrated at a frequency of 20 ± 0.5 kHz with an amplitude of 50 ± 0.5 µm peak-to-peak.

Two cavitation erosion tests were conducted: (i) in distilled water and (ii) in a water-sand mixture. For the water-sand mixture tests, silica sand with two different particle size ranges (50–100 µm and 200–400 µm) was added to the distilled water at a 3 kg/m^3 concentration. The sand particles were suspended using a miniature centrifugal pump installed in the test chamber.

The cavitation erosion tests were interrupted at predetermined intervals (1, 1, 2, 4, 8, 16, 32, and 32 min) to measure the mass loss of the samples. The samples were cleaned in an ultrasonic bath with

acetone, dried, and weighed using a precision balance with an accuracy of ±0.1 mg. The average mass loss from three samples was reported for each test condition.

2.4. Mud jet erosion testing

Mud jet erosion tests were carried out using a slurry jet erosion tester (DUCOM, India) following ASTM G73-10. The test samples (25 mm × 40 mm × 4.75 mm) were mounted on a specimen holder and subjected to a high-velocity jet of sand-water slurry. The slurry was prepared by mixing silica sand (particle size range: 200–400 μm) with water at a 3 kg/m³ concentration. The jet velocity was maintained at 25.5 m/s, and the nozzle diameter was 4 mm.

The impact angle of the mud blast varied at 3 different levels, 30°, 60°, and 90°, while all other parameters remained constant for all tests. **Figure 4** shows the positioning of the support at the different impact angles of the mud jet studied. Like the cavitation wear tests, mud blast tests were performed on duplicates of the Cr_3C_2 25NiCr, WC 10Co4Cr, and CA6NM steel coatings, thus totaling 18 samples due to the variation of the 3 impact angles. During the tests, after each time interval, the samples were cleaned, dried, and then weighed to obtain the curve of the behavior of the erosive wear by the mud jet.

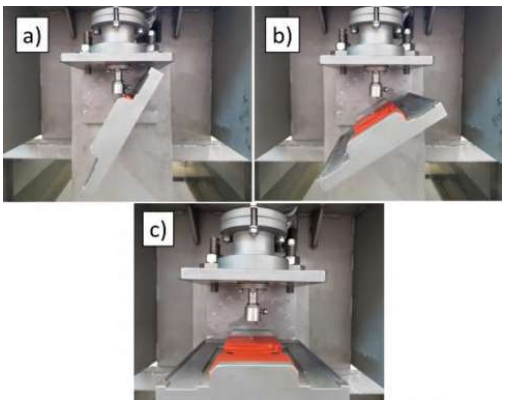

Figure 4. Support of the mud blast equipment positioned at the different angles of impact of the jet studied; **(a)** 30° impact angle; **(b)** 60° impact angle; **(c)** 90° impact angle.

Like cavitation wear tests, mud jet tests were carried out on duplicates of the Cr_3C_2 25NiCr coatings, WC 10Co4Cr, and CA6NM steel, thus totaling 18 samples due to variation in 3 impact angles. During the tests, after each time interval, the samples were cleaned, dried, and then weighed to obtain the erosive wear behavior curve by mud jet. The mud jet erosion tests were performed at three different impact angles (30°, 60°, and 90°) to investigate the effect of impact angle on the erosion behavior of the coatings. The tests were interrupted at predetermined intervals (30, 60, 120, 240, and 480 s) to measure the mass loss of the samples. The samples were cleaned, dried, and weighed using the same procedure as described for the cavitation erosion tests.

3. Experimental setup and procedure

3.1. HVOF thermal spraying

The Cr_3C_2-25NiCr and WC-10Co-4Cr coatings were deposited using a Diamond Jet DJ2700 HVOF thermal spray system. The HVOF system comprises a spray gun, gas supply unit, powder feeder, and a control console. The spray gun is equipped with a convergent-divergent nozzle that accelerates the combustion gases and the powder particles to supersonic velocities. The grit-blasted substrates were mounted 250 mm from the spray gun nozzle on a rotating turntable. The turntable was rotated at 150

rpm to ensure uniform coating deposition. The HVOF spraying parameters, as listed in **Table 2** of the manuscript, were kept constant for both coatings. The spraying process was carried out in an enclosed booth with a ventilation system to remove dust and fumes.

3.2. Coating characterization

The microstructure and porosity of the coatings were analyzed using a scanning electron microscope. The as-sprayed coatings were sectioned using a precision cutting machine with a diamond cutting wheel. The sectioned samples were mounted in epoxy resin and polished using a series of SiC abrasive papers (220, 600, and 1200 grit), followed by polishing with diamond suspensions (1 μm and 0.25 μm) to obtain a mirror-like surface finish. The SEM examined the polished cross-sections using secondary electron (SE) and backscattered electron (BSE) imaging modes. The SEM was operated at an accelerating voltage of 15 kV and a working distance of 15 mm. The porosity of the coatings was evaluated using image analysis techniques following ASTM E2109-01 (2014). SEM microfigures of the polished cross-sections were acquired at 500× magnification, and the area fraction of porosity was determined using the ImageJ software (National Institutes of Health, USA).

The phase composition of the coatings was investigated using X-ray diffraction (XRD) with a Bruker ECO D8 ADVANCE diffractometer (Bruker AXS GmbH, Germany) using Cu-Kÿ radiation (*ÿ* = 1.54 nm). The XRD patterns were acquired over a 2ÿ range of 20°–80° with a step size of 0.04° and a scan speed of 1°/min.

The microhardness of the coatings was measured on the polished cross-sections using a Vickers indenter with a load of 300 gf and a dwell time of 15 s. Ten indentations were made on each coating, and the average microhardness value was reported. The fracture toughness of the coatings was evaluated using the indentation crack length method. Vickers indentations were made on the polished cross-sections using a higher load of 10 kgf, and the crack lengths emanating from the indentation corners were measured using an optical microscope.

3.3. Cavitation erosion testing

Cavitation erosion tests were performed using an ultrasonic vibratory apparatus following ASTM G32. The test samples (25 mm × 40 mm × 4.75 mm) were mounted on a stationary specimen holder and immersed in distilled water maintained at a temperature of 25 ± 1 °C. The vibratory horn, with a diameter of 19 mm, was positioned above the sample surface at a distance of 500 μm. The horn vibrated at 20 ± 0.5 kHz with an amplitude of 50 ± 0.5 μm peak-to-peak.

The cavitation test seeks to evaluate the resistance of materials when subjected to the cavitation phenomenon. The most direct way to obtain such resistance It is by studying the mass loss of the material. The cavitation tests were performed using equipment from the Qsonica Q700 ultrasonic machine located in the Metallofigureic Preparation Laboratory of UTFPR-PG. The image of the equipment is shown in **Figure 5**.

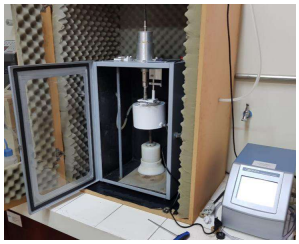

Figure 5. Cavitation test equipment.

Two cavitation erosion tests were conducted: (i) in distilled water and (ii) in a water-sand mixture. For the water-sand mixture tests, silica sand with two different particle size ranges (50–100 µm and 200–400 µm) was added to the distilled water at a 3 kg/m^3 concentration. The sand particles were suspended using a miniature centrifugal pump installed in the test chamber. The cavitation erosion tests were interrupted at predetermined intervals (1, 1, 2, 4, 8, 16, 32, and 32 min) to measure the mass loss of the samples. The samples were cleaned in an ultrasonic bath with acetone, dried, and weighed using a precision balance (Shimadzu AUX 220, Japan) with an accuracy of ±0.1 mg. The average mass loss from three samples was reported for each test condition.

The cavitation erosion rate (CER) was calculated using the following equation:

$$CER = (ÿm \times 10^6)/(ÿ \times A \times t)$$

where *ÿm* is the mass loss (g), *ÿ* is the density of the coating (g/cm^3), *A* is the surface area of the sample exposed to cavitation (cm^2), and *t* is the test duration (min).

3.4. Mud jet erosion testing

Mud jet erosion tests were carried out using a slurry jet erosion tester (DUCOM, India) following ASTM G73-10 (2017). The test samples (25 mm × 40 mm × 4.75 mm) were mounted on a specimen holder and subjected to a high-velocity jet of sand-water slurry. The slurry was prepared by mixing silica sand (particle size range: 200–400 µm) with water at a 3 kg/m^3 concentration. The jet velocity was maintained at 25.5 m/s, and the nozzle diameter was 4 mm.

Figure 6 shows the mud blasting machine and the support of the sample. The mud jet erosion tests were performed at three different impact angles (30°, 60°, and 90°) to investigate the effect of impact angle on the erosion behavior of the coatings. The tests were interrupted at predetermined intervals (30, 60, 120, 240, and 480 s) to measure the mass loss of the samples. The samples were cleaned, dried, and weighed using the same procedure as described for the cavitation erosion tests.

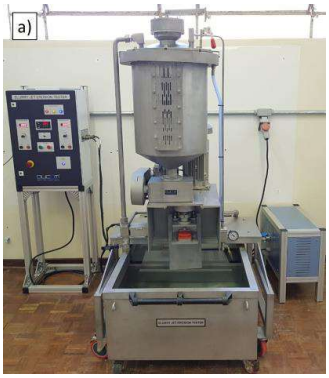

Figure 6. DUCOM Mud Jet Equipment used in erosive wear tests; **(a)** General image of the equipment.

The mud jet erosion rate (MJER) was calculated using the following equation:

$$MJER = (ÿm \times 10^6)/(ÿ \times A \times t)$$

where *ÿm* is the mass loss (g), *ÿ* is the density of the coating (g/cm^3), *A* is the surface area of the sample exposed to the mud jet (cm^2), and *t* is the test duration (min).

3.5. Wear mechanism analysis

After the cavitation and mud jet erosion tests, the worn surfaces of the coatings were examined using a scanning electron microscope to investigate the wear mechanisms. The samples were cleaned in an ultrasonic bath with acetone and dried before SEM analysis. The SEM was operated in secondary

electron (SE) imaging mode at an accelerating voltage of 15 kV and a working distance of 15 mm. The SEM microfigures were analyzed to identify the dominant wear mechanisms, such as microgrooving, carbide cracking, carbide detachment, and plastic deformation.

4. Results and discussion

The results obtained from characterizing the Cr_3C_2 25NiCr and WC 10Co4Cr coatings indicate that the Cr_3C_2 25NiCr coating had a lower porosity level of 1.67% compared to 3.95% for the WC 10Co4Cr coating. The average thickness of the coatings was very similar, around 220 µm. Analysis of the microstructure showed that the Cr_3C_2 carbides in the Cr_3C_2 25NiCr coating were larger compared to the finer WC carbides in the WC 10Co4Cr coating. XRD results confirmed the presence of Cr_3C_2 and Ni peaks in the Cr_3C_2 25NiCr coating, while WC, W2C, and Co peaks were observed for the WC 10Co4Cr coating.

4.1. Analysis of the microstructure and present phases of sprayed coatings

In order to characterize both coatings sprayed by HVOF, it was possible to define the percentage of porosity of the coatings, as well as the thickness of the deposited layer of Cr_3C_2 25NiCr and WC 10Co4Cr. **Figure 7** shows the microstructure of Cr_3C_2 25NiCr and WC 10Co4Cr coatings obtained in the cross-section of the samples. The figure shows the coating layer on the substrate, the proximity of the thickness of both coatings, and the high compaction of the coatings with the low presence of pores.

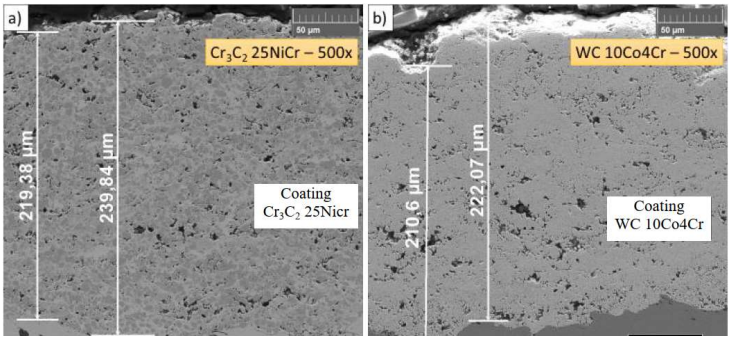

Figure 7. Cross-section of samples sprayed by HVOF; **(a)** Cr_3C_2 25NiCr; **(b)** WC 10Co4Cr.

The results of the porosity of both coatings show low pore levels, both below 4%, with the coating Cr_3C_2 25NiCr having a lower percentage of pores when compared to WC 10Co4Cr. In images of the microstructure at higher magnification, it is possible to identify the presence of carbides, matrix, and pores in the coatings (**Figure 8**).

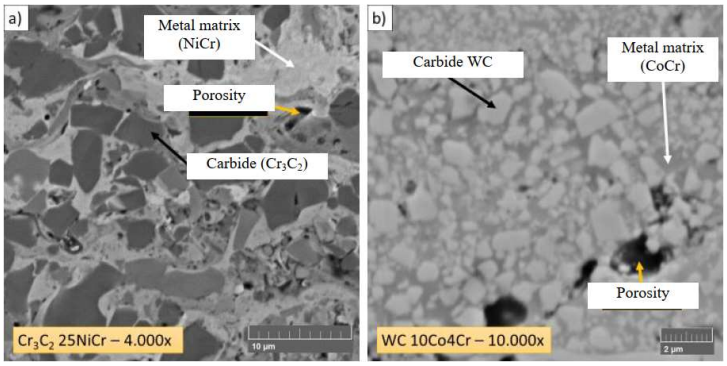

Figure 8. Microstructure of samples sprayed by HVOF; **(a)** Cr_3C_2 25NiCr; **(b)** WC 10Co4Cr.

In **Figure 8a**, Cr_3C_2 carbides are identified by the most dark; they are attached to the NiCr metallic matrix, which is identified as the clearer phase. The black dots present are identified as pores. For the 10Co4Cr WC coating, WC carbides, CoCr metal matrix, and pores are identified in **Figure 8b** but identified in opposite shades of gray, with high-density carbides highlighted in the image in lighter tones. It can be seen in the figure that, for both coatings, the carbide's hard materials are surrounded by the tenacious metallic matrix that acts as a binder in the coatings. Comparing both coatings, it is possible to notice the greater porosity of WC 10Co4Cr, as well as the highest percentage of metallic matrix of Cr_3C_2 25NiCr of 25% (WC 10Co4Cr with only 14%) found based on the chemical composition of the powder.

Regarding the size of the carbides in the coating, most of the carbides in the Cr_3C_2 25NiCr coating were between 4 and 10 ÿm. While the carbides found in the WC 10Co4Cr coating were much smaller, with the vast majority varying between 0.5 and 2 ÿm. Stands out the fact that smaller carbides and smaller amounts of metallic matrix of WC 10Co4Cr result in a smaller spacing between hard carbide particles and consequent greater phase distribution when compared to Cr_3C_2 25NiCr.

In addition to analyzing the microstructure of the coatings, the phases present in each sprayed coating were evaluated with the aid of the DRX equipment. **Figure 9** shows the diffractograms of the coating surfaces of Cr_3C_2 25NiCr and WC 10Co4Cr.

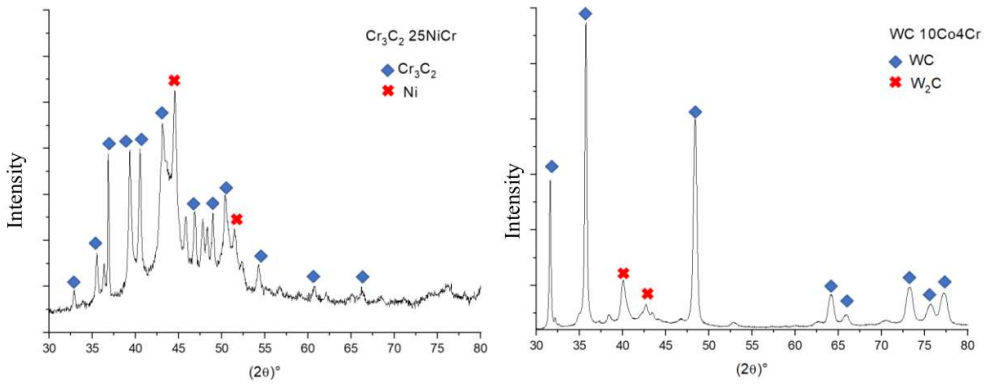

Figure 9. Diffractograms obtained by XRD of the different sprayed coatings; **(a)** Cr_3C_2 25NiCr; **(b)** WC 10Co4Cr.

Several Cr_3C_2 peaks were observed in the Cr_3C_2 25NiCr coating, which indicates the retention of a large part of the carbides during the coating deposition. Ni peaks were also observed in **Figure 9a**, as highlighted with great intensity at the 44° angle. Other carbides like Cr7C3 and Cr23C6 were not observed in the coating diffractogram. WC and W2C were observed in **Figure 9b** of the coating WC 10Co4Cr. The formation of the W2C phase indicates that the coating has undergone decarburization during the deposition process; the presence of this phase in the material can influence the properties of the coating, such as hardness and weathering toughness—fracture due to the formation of these brittle carbides.

4.2. Analysis of resistance to cavitation wear

Among both sprayed materials, the coating with the highest cavitation wear resistance was Cr_3C_2 25NiCr. **Figure 10** shows the cavitation mass loss curve of the Cr_3C_2 25NiCr and WC 10Co4Cr coatings, highlighting the behavior of cavitation wear at different time intervals.

Because of the difference in density between the Cr_3C_2 25NiCr and WC 10Co4Cr coatings, it is also important to highlight the volumetric loss behavior of both coatings. Thus, **Figure 11** shows the volumetric wear of Cr_3C_2 25NiCr and WC 10Co4Cr under the effect of cavitation.

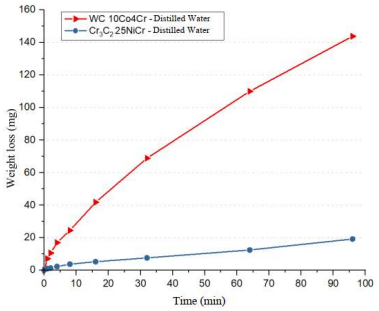

Figure 10. Cavitation mass loss of Cr_3C_2 25NiCr and WC 10Co4Cr coatings.

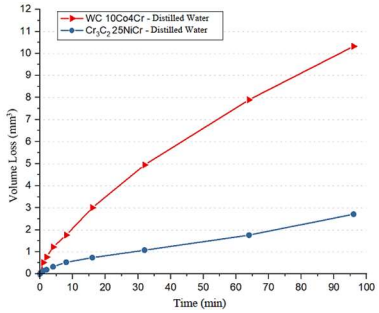

Figure 11. Volume loss due to cavitation of Cr_3C_2 25NiCr and WC 10Co4Cr coatings.

If we compare **Figures 12** and **13**, it can be seen that when analyzing the behavior of cavitation wear in volumetric terms, we have an approximation of the curves, thus reducing the difference in resistance between the coatings; however, it is important to highlight the greater resistance of the Cr_3C_2 25NiCr coating in terms of cavitation resistance. According to **Figure 13**, it is noted that both coatings did not present an incubation period; the same was observed in the literature. The coatings suffered mass loss from the beginning of the test and showed a more intense wear rate in the first 8 min. After this interval, the liners showed a linear evolution of cavitation wear until the end of the tests, thus generating a particular cavitation wear rate for each. The Cr_3C_2 25NiCr coating generally showed a much lower wear curve inclination than the WC 10Co4Cr.

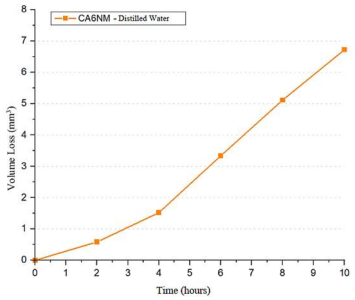

Figure 12. Volume loss due to cavitation of CA6NM steel.

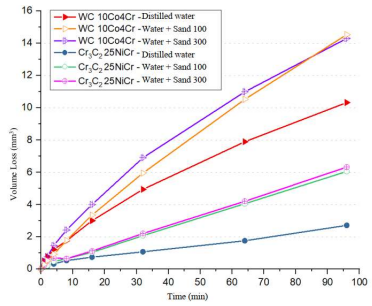

Figure 13. Volume loss of Cr_3C_2 25NiCr and WC 10Co4Cr coatings in the fluid cavitation process with and without sand.

Thus, it can be stated that the wear rate of Cr_3C_2 25NiCr is lower and, therefore, has greater resistance to cavitation. Notably, the Cr_3C_2 25NiCr coating with higher fracture toughness and lower porosity level in the coating presented better cavitation resistance results. For CA6NM steel with much higher fracture toughness than the coatings studied here, as well as the low pore percentage of the cast alloy, the behavior of the steel in the cavitation tests was more resistant to the cavitation phenomenon. The figure shows the results of cavitation wear of CA6NM steel. Within the first 4 h of the cavitation assay, a slight volume variation indicated that the CA6NM steel was within the cavitation process's incubation period. Between 4 and 10 h of testing, the behavior of the volumetric loss by cavitation of the CA6NM steel intensified, maintaining a wear rate of 0.9 mm^3/h. This rate was lower when compared to the sprayed coatings, thus demonstrating the higher cavitation resistance of CA6NM steel. Among the different variations of sand microparticles in the fluid and deposited coatings, the sample that showed the best resistance to cavitation wear was Cr_3C_2 25NiCr when submitted to the cavitation test with pure distilled water, without adding sand. On the other hand, the sample that presented the lowest resistance to cavitation wear was WC 10Co4Cr, which was submitted to the sand cavitation test.

For both coatings, there is a very distinct behavior between the wear curves of the specimens subjected to sand and sand cavitation tests. While the curves of the tests with sand 100 and sand 300 showed very similar behaviors, it cannot be said that there was a variation in wear among the different sands studied. All the curves in **Figure 13**, including the coatings tested with the addition of sand, did not present an incubation period, suffering volume loss from the beginning of the test with a more intense wear rate in the first 8 minutes of the test, and then a linear evolution of wear by cavitation until the end of the tests. The Cr_3C_2 25NiCr coating exhibited a higher average microhardness of 824 HV compared to 853 HV for the WC 10Co4Cr coating; however, the high standard deviation meant there was no statistically significant difference between the hardness values. In contrast, the fracture toughness of Cr_3C_2 25NiCr at 4.6 MPa.m1/2 was higher than the 3.2 MPa.m1/2 for WC 10Co4Cr. The higher metallic matrix content and lower porosity level of the Cr_3C_2 25NiCr coating likely contributed to its greater fracture toughness.

In the cavitation wear tests, the Cr_3C_2 25NiCr coating demonstrated higher resistance than the WC 10Co4Cr coating in tests with pure water and with sand addition. The Cr_3C_2 25NiCr coating showed an incubation period before steady-state wear, while the WC 10Co4Cr coating suffered material loss right from the start. Adding sand resulted in a 260% increase in wear rate for Cr_3C_2 25NiCr and a 40% increase for WC 10Co4Cr, indicating the synergistic effect of cavitation and erosion in sand slurry. The higher fracture toughness and lower porosity level of Cr_3C_2 25NiCr are likely responsible for its superior cavitation resistance compared to WC 10Co4Cr. Wear mechanisms involved microcracking, pore damage, and carbide detachment.

Mud jet erosion tests showed the opposite trend, with the WC 10Co4Cr coating demonstrating higher resistance than Cr_3C_2 25NiCr at all impingement angles. The maximum wear rate occurred at 30° for the coatings and 90° for the CA6NM steel. The improved erosion resistance of WC 10Co4Cr is attributed to the fine, uniformly dispersed carbides compared to the larger Cr_3C_2 particles. At shallow impingement angles, mechanisms like carbide cracking and micro grooving of the matrix were more prevalent. The ductile CA6NM steel underwent plastic deformation and grooving as the primary wear mechanism.

The results demonstrate the complex interplay between material properties like fracture toughness, porosity, carbide size/distribution, and matrix content in influencing cavitation and erosion behaviors.

The test parameters, including sand concentration, impingement angle, and exposure time, provide additional variables determining the wear rate and mechanisms.

5. Conclusions

The Cr_3C_2 25NiCr and WC 10Co4Cr thermal spray coatings fabricated by HVOF exhibited differences in their resistance to cavitation and erosion wear. The key findings are:

- Cr_3C_2 25 NiCr had lower porosity (1.67%) than WC 10Co4Cr (3.95%) and higher fracture toughness (4.6 MPa.m1/2) compared to WC 10Co4Cr (3.2 MPa.m1/2).
- In cavitation tests, Cr_3C_2 25 NiCr showed higher resistance, attributed to its fracture toughness and lower porosity. Adding sand particles increased the wear rate significantly.
- WC 10Co4Cr demonstrated superior resistance to mud jet erosion due to its fine, uniformly distributed carbides. Maximum wear occurred at a shallow 30° impingement angle.
- Depending on test conditions, wear mechanisms included microcracking, carbide detachment, pore damage, microgrooving, and plastic deformation.
- Material properties like fracture toughness, porosity, carbide size/distribution, and matrix content interacted in complex ways to determine cavitation and erosion behaviors.
- Test parameters such as sand concentration, jet angle, and exposure duration strongly influenced the measured wear rates and mechanisms.

Author contributions

Conceptualization and methodology, ADH; data analysis and writing the manuscript, RD. All authors have read and agreed to the published version of the manuscript.

Conflict of interest

The authors declare no conflict of interest.

References

1. Amarendra HJ, Prathap MS, Karthik S, et al. Combined Slurry and Cavitation Erosion Resistance of Hvof Thermal Spray Coated Stainless Steel. Materials Today: Proceedings. 2017; 4(2): 465-470. doi: 10.1016/j.matpr.2017.01.046
2. Ding X, Cheng X, Yu X, et al. Structure and cavitation erosion behavior of HVOF sprayed multi-dimensional WC-10Co4Cr coating. Transactions of Nonferrous Metals Society of China. 2018; 28(3): 487-494. doi: 10.1016/S1003-6326(18)64681-3
3. Ding X, Huang Y, Yuan C, et al. Deposition and cavitation erosion behavior of multimodal WC-10Co4Cr coatings sprayed by HVOF. Surface and Coatings Technology. 2020; 392: 125757. doi: 10.1016/j.surfcoat.2020.125757
4. Ding Z, Chen W, Wang Q. Resistance of cavitation erosion of multimodal WC-12Co coatings sprayed by HVOF. Transactions of Nonferrous Metals Society of China. 2011; 21(10): 2231-2236. doi: 10.1016/S1003-6326(11)61000-5
5. Hong S, Mei D, Wu J, et al. Hydro-abrasive erosion and cavitation-silt erosion characteristics of HVOF sprayed WC-Ni cermet coatings under different flow velocities and sand concentrations. Ceramics International. 2023; 49(1): 74–83. doi: 10.1016/j.ceramint.2022.08.282
6. Hong S, Shi X, Lin J, et al. Microstructure and cavitation-silt erosion behavior of two HVOF-sprayed hardfacing coatings for hydro-turbine applications. Alexandria Engineering Journal. 2023; 69: 483-496. doi: 10.1016/j.aej.2023.02.010
7. Hong S, Wei Z, Lin J, et al. Cavitation-silt erosion behavior and mechanism in simulated sea water slurries of cermet coatings manufactured by HVOF spraying. Ceramics International. 2023; 49(9): 14355-14366. doi: 10.1016/j.ceramint.2023.01.024

8. Jonda E, Szala M, Sroka M, et al. Investigations of cavitation erosion and wear resistance of cermet coatings manufactured by HVOF spraying. Applied Surface Science. 2023; 608: 155071. doi: 10.1016/j.apsusc.2022.155071
9. Kanno A, Takagi K, Arai M. Influence of chemical composition, grain size, and spray condition on cavitation erosion resistance of high-velocity oxygen fuel thermal-sprayed WC cermet coatings. Surface and Coatings Technology. 2020; 394: 125881. doi: 10.1016/j.surfcoat.2020.125881
10. Kumar H, Chittosiya C, Shukla VN. HVOF Sprayed WC Based Cermet Coating for Mitigation of Cavitation, Erosion & Abrasion in Hydro Turbine Blade. Materials Today: Proceedings. 2018; 5(2): 6413-6420. doi: 10.1016/j.matpr.2017.12.253
11. Kumar V, Singh V, Verma R, et al. Cavitation-corrosion analysis of HVOF-sprayed WC-Co-Cr-graphene nanoplatelets coatings with LST pre-treatment. International Journal of Refractory Metals and Hard Materials. 2024; 120: 106610. doi: 10.1016/j.ijrmhm.2024.106610
12. Lamana MS, Pukasiewicz AGM, Sampath S. Influence of cobalt content and HVOF deposition process on the cavitation erosion resistance of WC-Co coatings. Wear. 2018; 398-399: 209-219. doi: 10.1016/j.wear.2017.12.009
13. Lekatou AG, Sioulas D, Grimanelis D. Corrosion and wear of coatings fabricated by HVOF- spraying of nanostructured and conventional WC–10Co-4Cr powders on Al7075-T6. International Journal of Refractory Metals and Hard Materials. 2023; 112: 106164. doi: 10.1016/j.ijrmhm.2023.106164
14. Lin J, Hong S, Zheng Y, et al. Cavitation erosion resistance in NaCl medium of HVOF sprayed WC-based cermet coatings at various flow velocities: A comparative study on the effect of Ni and CoCr binder phases. International Journal of Refractory Metals and Hard Materials. 2021; 94: 105407. doi: 10.1016/j.ijrmhm.2020.105407
15. Maekai IA, Harmain GA, Din ZU, et al. Resistance to Slurry Erosion by Wc-10co-4cr and Cr3C2-25(Ni20cr) Coatings Deposited by Hvof Stainless Steel F6nm. International Journal of Refractory Metals and Hard Materials. 2022; 105: 105830. doi: 10.1016/j.ijrmhm.2022.105830
16. Pattnayak A, Gupta A, Abhijith NV, et al. Development of rGO doped alumina-based wear and corrosion resistant ceramic coatings on steel using HVOF thermal spray. Ceramics International. 2023; 49(11): 17577-17591. doi: 10.1016/j.ceramint.2023.02.124
17. Ribu DC, Rajesh R, Thirumalaikumarasamy D, et al. Experimental investigation of erosion corrosion performance and slurry erosion mechanism of HVOF sprayed WC-10Co coatings using design of experiment approach. Journal of Materials Research and Technology. 2022; 18: 293-314. doi: 10.1016/j.jmrt.2022.01.134
18. Ribu DC, Rajesh R, Thirumalaikumarasamy D, et al. Influence of rotational speed, angle of impingement, concentration of slurry and exposure time on erosion performance of HVOF sprayed cermet coatings on 35CrMo steel. Materials Today: Proceedings. 2021; 46: 7518-7530. doi: 10.1016/j.matpr.2021.01.307
19. Shi X, Cui D, Wei Z, et al. The influence of sulphide on the ultrasonic cavitation erosion-corrosion behaviors of HVOF-sprayed WC-Cr3C2-Ni coating. Ultrasonics Sonochemistry. 2023; 100: 106629. doi: 10.1016/j.ultsonch.2023.106629
20. Singh NK, Ang ASM, Mahajan DK, Singh H. Cavitation erosion resistant nickel-based cermet coatings for monel K-500. Tribology International. 2021; 159: 106954. doi: 10.1016/j.triboint.2021.106954
21. Singh NK, Vinay G, Ang ASM, et al. Cavitation erosion mechanisms of HVOF-sprayed Ni-based cermet coatings in 3.5% NaCl environment. Surface and Coatings Technology. 2022; 434: 128194. doi: 10.1016/j.surfcoat.2022.128194
22. Singh V, Singh I, Bansal A, et al. Cavitation erosion behavior of high velocity oxy fuel (HVOF) sprayed (VC + CuNi-Cr) based novel coatings on SS316 steel. Surface and Coatings Technology. 2022; 432: 128052. doi: 10.1016/j.surfcoat.2021.128052
23. Vaz RF, Silveira LL, Cruz JR, et al. Cavitation resistance of FeMnCrSi coatings processed by different thermal spray processes. Hybrid Advances. 2024; 5: 100125. doi: 10.1016/j.hybadv.2023.100125
24. Wei Z, Wu Y, Hong S, et al. Effect of WC-10Co on cavitation erosion behaviors of AlCoCrFeNi coatings prepared by HVOF spraying. Ceramics International. 2021; 47(11): 15121-15128. doi: 10.1016/j.ceramint.2021.02.070
25. Xiao M, Nai S, Nan S, et al. Preparation, mechanical properties and wear resistance of dual-sized TiC particles reinforced high-entropy alloy cermet coating. Journal of Materials Research and Technology. 2024; 28: 97–109. doi: 10.1016 /j.jmrt.2023.11.264